

Contents lists available at [ScienceDirect](https://www.sciencedirect.com)

# Journal of Sound and Vibration

journal homepage: [www.elsevier.com/locate/jsvi](http://www.elsevier.com/locate/jsvi)

## Planar Swirl-shaped Acoustic Black Hole Absorbers for Multi-directional Vibration Suppression

Tong Zhou, Li Cheng\*

*Department of Mechanical Engineering, The Hong Kong Polytechnic University, Hong Kong*

### ABSTRACT

A planar swirl-shaped Acoustic Black Hole (ABH) absorber is proposed and investigated in this paper. In addition to the well-known bending wave retarding phenomena, the speed of torsional waves in the curved ABH with a rectangular cross section is also shown to decrease with the thickness thinning. Alongside the enhanced bending-twisting coupling brought about by the planar and curvilinear configuration, the curved ABH absorber exhibits reduced orientation-dependent properties to cope with multi-directional rotational moment excitations, and meanwhile generates enriched dynamics and enhanced energy trapping and dissipation. As a result, the absorber enables broadband multi-directional vibration suppression when added on a primary thin structure. Experimental studies demonstrate that deploying multiple distributed ABH absorbers can entail effective, robust and broadband vibration reduction for an arbitrarily selected polygon plate. Analyses also confirm the dual vibration reduction mechanisms in terms of structural interaction and damping enhancement, both being fully played out through the proposed curvilinear ABH design.

### 1. Introduction

In recent years, a newly emerging wave phenomenon called Acoustic Black Hole (ABH) has shown great promise for vibration and noise control applications [1]. The realization of the ABH effect is based on the properties of flexural wave propagation in a beam or plate structure with a reducing thickness tailored according to a power function. It is shown that flexural waves undergo slow-down in propagation when travelling towards the thin structural section [2, 3] to generate highly localized and strong oscillations, where efficient energy absorption can be achieved with minimal surface damping treatment [4, 5]. Conventional ABHs take the form of a tapered wedge-like beam or slot/circular indentations embedded in a plate [3]. Resulted ABH features have been studied from different perspectives such as wave attenuation [6, 7], vibration control [8], energy isolation [9-11], sound radiation reduction [12, 13] and energy harvesting [14-16] etc. Meanwhile, exploration of potential applications of the ABH-based technology is on-going with good progress made with resort to system design and optimization [17, 18].

Recently, we have proposed an ABH-based beam absorber as an add-on device to a primary structure for its vibration control [19]. By capitalizing on the remarkable ABH-induced wave trapping ability and rich dynamics, the proposed device embraces the working principles of both dynamic vibration absorbers (DVA) [20] and waveguide absorbers (WGA) [21]. The ABH beam absorber was shown to enable broadband suppression of resonant peaks of a host beam through either structural interaction or damping enhancement. Owing to the robust ABH effects, the delicate parameter tuning process, which is commonly required in conventional DVAs, can be avoided. The utilization of ABHs as an add-on vibration suppression device shows attractiveness, since in practice it is often not permissible to integrate local inhomogeneity into an existing structure, which inevitably compromises its rigidity and integrity [22]. However, as reviewed in Refs. [1, 23], there are fewer research advances on the add-on ABHs, as compared with the embedded configuration.

\* Corresponding author.

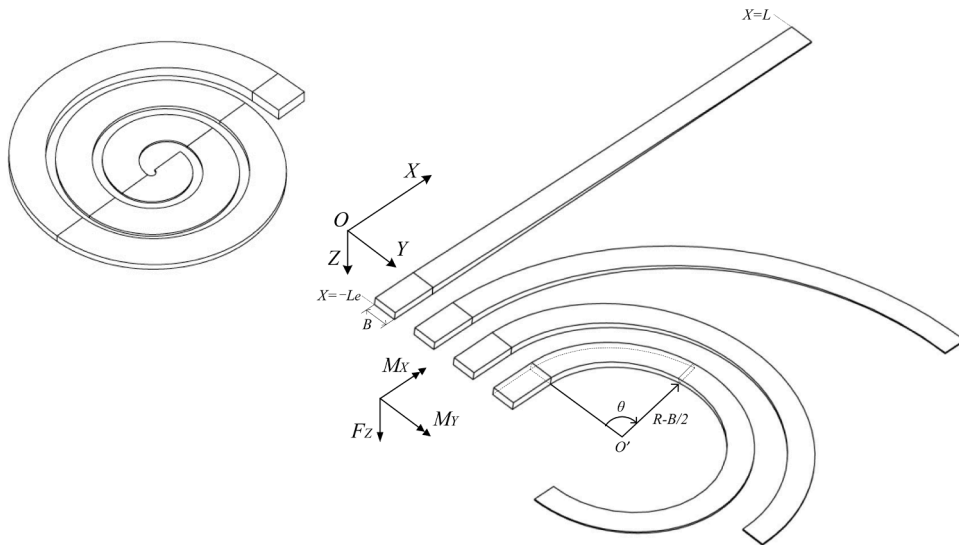
E-mail address: [li.cheng@polyu.edu.hk](mailto:li.cheng@polyu.edu.hk) (L. Cheng).

<https://doi.org/10.1016/j.jsv.2021.116500>

Received 26 April 2021; Received in revised form 12 August 2021; Accepted 26 September 2021

Available online 28 September 2021

0022-460X/© 2021 Elsevier Ltd. All rights reserved.



**Fig. 1.** Planar swirl-shaped ABH design in a coiled form (left) and circular arc form (right). The circular arc or C-shaped ABHs have the same length as the straight one. A damping layer can be coated on the structural surface.

Our previous work [19] investigated a one-dimensional primary structure coupled with a straight ABH beam for proof-of-concept studies. Despite the illustration of its efficacy, 1D beam-type ABHs show strong orientation-dependent properties to cope with multi-directional rotational excitations, in addition to their bulky dimension. For better space occupation efficiency [24, 25], which is also of great concern for other mechanical sub-systems [26, 27], existing spiral/helix design partly addresses the compactness issue, but does not resolve the orientation-dependent problem when used as an absorber. The problem becomes crucial when dealing with two-dimensional vibration field such as in a plate, where waves propagate along various directions simultaneously. In a broad sense, beam-type ABHs are mostly employed for attenuating flexural vibrations in one coordinate direction [28, 29], and the dependence of their energy propagation and absorption on multi-spatial directions deserves more systematic examination. Meanwhile, suitable absorber layout for achieving satisfactory vibration reduction, similar to the traditional add-on devices such as DVA and WGA [30-33], also deserves deeper examination. Recently, encouraging effort has been made by investigating an ABH disc absorber [34]. However, the highly selective coupling between the disc absorber and the host structure was shown to compromise the control performance.

In this work, a planar swirl-shaped ABH absorber is proposed, which is shown to generate novel physical phenomena, in terms of torsional wave propagation and bending-twisting coupling, that have not received due attention up to now in existing ABH studies. The swirl-shaped ABH absorber is formed by flexing and coiling a straight slender tapered beam into a curved shape, in a reference plane perpendicular to the beam thickness-wise direction, i.e.  $XY$  plane in Fig. 1. The proposed design offers a thin, compact and lightweight modular component that can be deployed as a localized addition over a two-dimensional primary structure for its vibration reduction. Note the reference plane selected to form the swirl-shaped ABH is different from that of the existing spiral ABHs in Refs. [24, 35, 36] ( $XZ$  plane in Fig. 1). The proposed design is later shown to incite new physical process in its local dynamics, which is conducive to achieving good, robust and broadband vibration reduction performance.

Before its embodiment with a host structure, numerical analyses are first conducted to investigate the dynamic and damping properties of a swirl-shaped ABH module, with particular focus on the curvature-induced effects. The wave deceleration phenomenon is examined. In addition to the well-known bending wave retarding phenomena, the speed of torsional waves in the curved ABH with a rectangular cross section is also shown to decrease with the thickness thinning. Meanwhile, the curvilinear ABH design enables enhanced bending-twisting coupling. Vibrational power flow analyses allow evaluating the capacities of curved ABHs in capturing and admitting mechanical energy injected by multi-directional rotational excitations, i.e.  $M_x, M_y$  acting on the thick end of an ABH shown in Fig. 1. To demonstrate their usability and working effectiveness, ABH absorbers incorporating curvilinear ABH features are installed over an arbitrarily selected polygon plate, which represents a generic two-dimensional structure. The vibration reduction performance and the underlying physical mechanisms are studied via assessing the frequency response functions, alongside an examination on the robustness of multiple discrete ABH devices through changing their number and positions. Owing to the add-on principle and curvilinear features, the proposed ABH absorbers are scalable for controlling plate vibrations under dynamic excitations in different frequencies ranges.

The rest of the paper is organized as follows. In Section 2, after depicting the configurations of the planar swirl-shaped ABHs, finite element (FE) simulations are carried out to analyse their modal properties and wave compression effects. Then we examine the orientational dependence of the ABH in terms of trapping input mechanical power and its relationship with the curvature. Section 3 presents a series of experimental studies on the performance of the swirl-shaped ABH absorbers when installed on a polygon plate. Conclusions are drawn in the final section.

**Table 1**  
Parameters used in simulations.

Geometrical parameters	Material parameters	
$H_0 = 0.0005$ m	Aluminium structure	
$\varepsilon = 0.003$ m <sup>-1</sup>	$E = 70$ GPa	$\rho = 2700$ kg/m <sup>2</sup>
$L = 0.2$ m	$G = 27$ GPa	$\eta = 0.1\%$
$B = 0.01$ m	Damping layer	
$H_d = 0.001$ m	$E = 60$ MPa	$\rho = 980$ kg/m <sup>2</sup>
$L_e = 0.02$ m	$G = 20$ MPa	$\eta = 0.9$

## 2. Planar swirl-shaped ABH

### 2.1. Description of configuration

Consider a straight slender wedge-like structure with a rectangular cross section in Fig. 1. The bottom surface lies in the  $XY$  plane and the baseline is defined to coincide with its midline along the lengthwise direction. The straight ABH wedge is tailored with a thickness (or height) profile according to the following power function:

$$H(x) = \varepsilon(x - L)^2/L^2 + H_0, \text{ where } 0 \leq x \leq L \quad (1)$$

where  $\varepsilon$  is a constant;  $H_0$  the residual thickness and  $L$  the length of the wedge. The wedge has a constant width  $B$  and a uniform portion is extracted from the thick termination of the tapered portion by a length  $L_e$  for connection purposes. The key ingredient of the ABH effect relies on the dependence of the bending wave speed,  $C_B$ , on the geometric parameters as:

$$C_B = \omega^{1/2} \left( \frac{EI}{\rho S} \right)^{1/4} = \omega^{1/2} \left( \frac{EH^2}{12\rho} \right)^{1/4}, \quad (2)$$

where  $I$  is the second moment of area;  $S$  the cross-sectional area;  $\omega$  the angular frequency;  $E$  Young's modulus and  $\rho$  the density.

A curved ABH can then be formed by modifying the straight baseline ( $y = 0$ ) to a circular arc of a constant radius  $R$

$$x = R\sin\theta, \quad y = R - R\cos\theta. \quad (3)$$

Here,  $0 \leq \theta \leq L/R$ , the centre of the circular baseline  $O'$  is at  $(0, R)$  and  $x$  and  $y$  are in the same orientations as the global coordinates  $X$  and  $Y$  in Fig. 1. The thickness profile of a circular arc ABH can then be expressed in a polar coordinate as

$$H(\theta) = \varepsilon(R\theta - L)^2/L^2 + H_0. \quad (4)$$

A damping layer of thickness  $H_d$  is bonded on the flat surface of the ABHs for vibrational energy dissipation.

To develop a coiled ABH, the arc radii for coiling are set to be variable (piecewise constant in this work) over the trajectory of the curvilinear baseline. This allows to use a longer taper length while maintaining compactness. The ABH in a planar coil can be viewed as a more general form of the swirl-shaped ABHs. These ABH components can be installed on a 2D primary thin structure through cementing or riveting. Note the curvilinear feature together with the add-on principle makes the planar swirl-shaped ABHs scalable for controlling structural responses in different frequencies ranges.

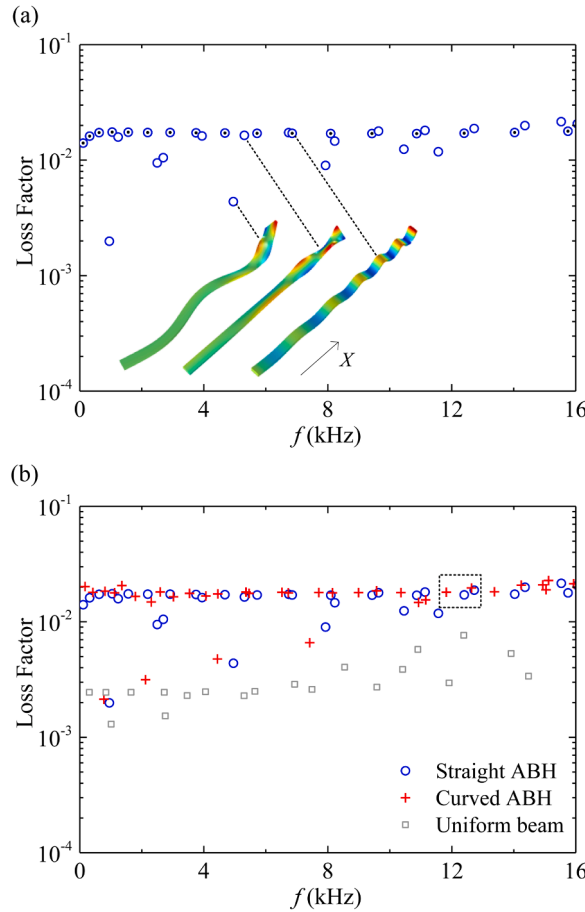
### 2.2. Dynamic analyses

The vibrational properties of the ABH module are investigated through finite element (FE) simulations before it is installed and coupled to a host structure. Analyses focus on the dynamics and damping of the planar swirl-shaped ABH modules. These are key factors which affect the vibration-reduction performance of the device in terms of dynamic interactions (typical of DVA) and waveguide absorption (typical of WGA).

Most previous works on wedge-like ABHs adopt the 1D beam bending model [37] or 2D plane stress elements [22, 38]. Here, we employ the 3D tetrahedron elements with quadratic discretization, which involve less assumptions for a more comprehensive analysis. FE simulations were carried out using Solid Mechanics Module in COMSOL Multiphysics<sup>TM</sup>. A similar FE model has been built for validation purposes in a previous work [22]. The simulation tool allows the use of a good mesh quality with a low element growth rate and the resolution of the mesh was chosen to be sufficiently fine to capture the fine details of vibrations in thin tapered portions. A convergence test was conducted with mesh refinement to check the reliability of the computed results. Eigen-frequencies and mode shapes of the ABH modules were first calculated, followed by forced harmonic responses by using the modal superposition approach.

In the following numerical simulations, we focus on the dynamic analyses of circular arc ABH form, owing to its simple configuration, allowable systematic comparison and reasonable computational cost. As shown in Fig. 1, the C-shaped ABHs with three arc angles are investigated, namely C-90, C-180 and C-270 (the numbers refer to angles in degrees). Table 1 tabulates the geometrical and material parameters of metallic ABHs and the damping layer coated on their flat surface.

Fig. 2(a) shows the system loss factors and the associated mode shapes of the straight ABH. This conventional ABH structure offers




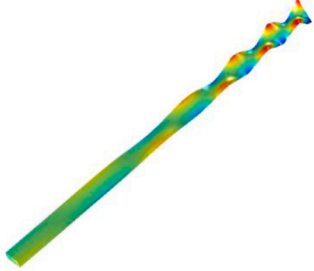
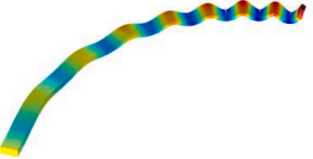
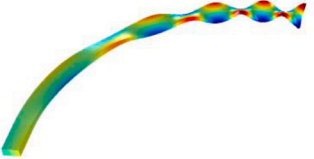
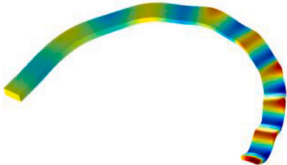

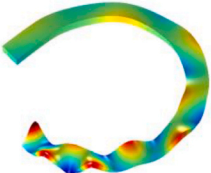
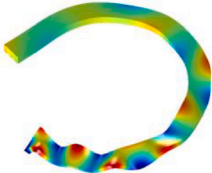
**Fig. 2.** (a) Loss factors and mode shapes of a straight ABH. The ABH bending modes are marked with centre dots and the displacement in Z-axis is shown with the rainbow colour. (b) comparisons of loss factors of straight and curved ABHs (C-180) with a uniform beam. All are free of constraints and rigid body modes are not given.

rich resonant modes and high modal damping, which is advantageous to be utilized as an auxiliary device for vibration control. Three typical modes are found: bending modes in the two principal planes and torsional modes. The bending wave motion in XZ plane is referred to as the so-called ABH phenomenon [3, 37], evidenced by shortened local wavelength and increased wave amplitude due to the wave deceleration with thickness reduction. A branch of modes, starting from relatively low loss factors at low frequencies, dominates the bending deformation in XY plane, which is called ‘lateral bending’ in this work. There is a little variation in the flexural wavelength and the vibration amplitude increases along X axis. The lateral bending is coupled with the twisting motion, more significantly near the wedge termination at higher frequencies. This results in an enhancement in system damping. A considerable number of torsional modes appear systematically in a broad frequency range. Each cross section of the taper rotates with an angular displacement with respect to the lengthwise direction (X axis) [39]. One can observe that the torsional wavelength becomes shorter and oscillation magnitude becomes larger as the cross-section area (thickness) diminishes. The torsional wave speed is dependent on the shape and the dimension of the cross section. A detailed explanation will be given in later part of this section. In this particular case, the fundamental frequency of the torsional modes is 1238Hz, while the first natural frequency of ABH-type bending modes is 111Hz. These two types of modes consistently appear. The lateral bending and torsional modes are coupled near 2500Hz. Note one longitudinal mode also appears at 10459Hz at which no wave compression effect is found, as expected.

Fig. 2(b) compares the modal properties of straight ABH and circular arc ABH C-180. It can be seen that the two ABH designs basically have close modal distribution and damping level in various frequency ranges. Similar comparisons can be made if the ABH C-180 is replaced by C-90 or C-270 and the results are not shown here for simplicity. Therefore, the introduction of curvature does not have a detrimental effect on structural dynamics and the damping brought by ABHs. Circular arc ABHs possess similar types of vibration modes as the straight one and they are capable of maintaining the wave compression and amplification effects induced by structural inhomogeneity, as illustrated in Table 2. Curved ABHs C-90 and C-180 exhibit modal responses dominated by ABH-related bending waves or torsional waves. These two types of vibration modes appear most frequently, which can be regarded as mode pairs. A larger curvature (C-270) can lead to a stronger coupling between the bending and twisting deformations and the curved ABH exhibits strong coupled vibrational behaviours in this case. More detailed explanations are given in the following power flow analyses. Fig. 2(b)

**Table 2**

Mode shapes of the straight and curved ABHs around 12 kHz, corresponding to the dash box area in Fig. 1(b) (Rainbow colour legend depicts displacement in Z direction).

 <p style="text-align: center;"><math>f_n=12402\text{Hz}</math></p>	 <p style="text-align: center;"><math>f_n=12725\text{Hz}</math></p>
 <p style="text-align: center;"><math>f_n=12013\text{Hz}</math></p>	 <p style="text-align: center;"><math>f_n=12435\text{Hz}</math></p>
 <p style="text-align: center;"><math>f_n=11823\text{Hz}</math></p>	 <p style="text-align: center;"><math>f_n=12638\text{Hz}</math></p>
 <p style="text-align: center;"><math>f_n=12857\text{Hz}</math></p>	 <p style="text-align: center;"><math>f_n=13153\text{Hz}</math></p>

also shows the modal properties of a uniform beam (or a space frame element, see Ref. [40]), which has the same length, width and thickness (uniform portion) as the straight ABH wedge with the same damping treatment. The uniform beam without ABH features possesses fewer modes with low loss factors. Such a beam cannot be exploited as a very efficient vibration-suppressing device, in views of creating effective dynamic coupling and wave trapping effects, as demonstrated in Ref. [19].

The analysis of wave propagation speed plays a fundamental role in the study of flexural vibrations of ABH-tailored structures. To explain the aforementioned torsional wave phenomena, we carry out a similar analysis for torsional waves based on the Saint-Venant theory or simple torsion theory [39, 41]. Here, a slender straight ABH wedge without a damping layer is considered. For a bar with noncircular cross section, its cross section undergoes rotations and warping during twisting oscillations. The phase velocity of the torsional waves in a rectangular bar of a thickness  $H$  and a width  $B$  is given by

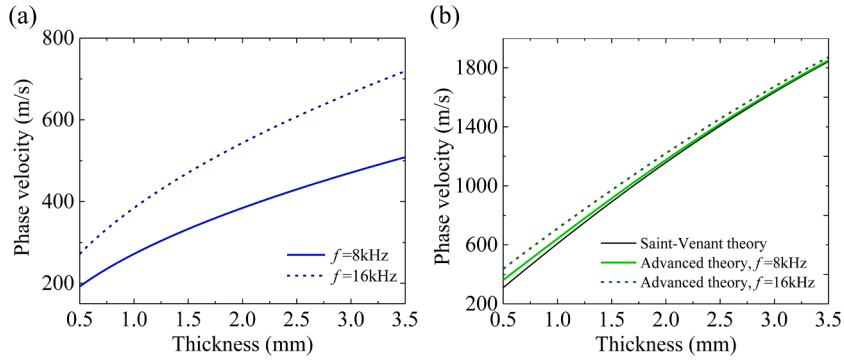


Fig. 3. Phase velocities of (a) bending waves and (b) torsional waves in a rectangular bar at each slice of the straight ABH wedge without damping treatment.

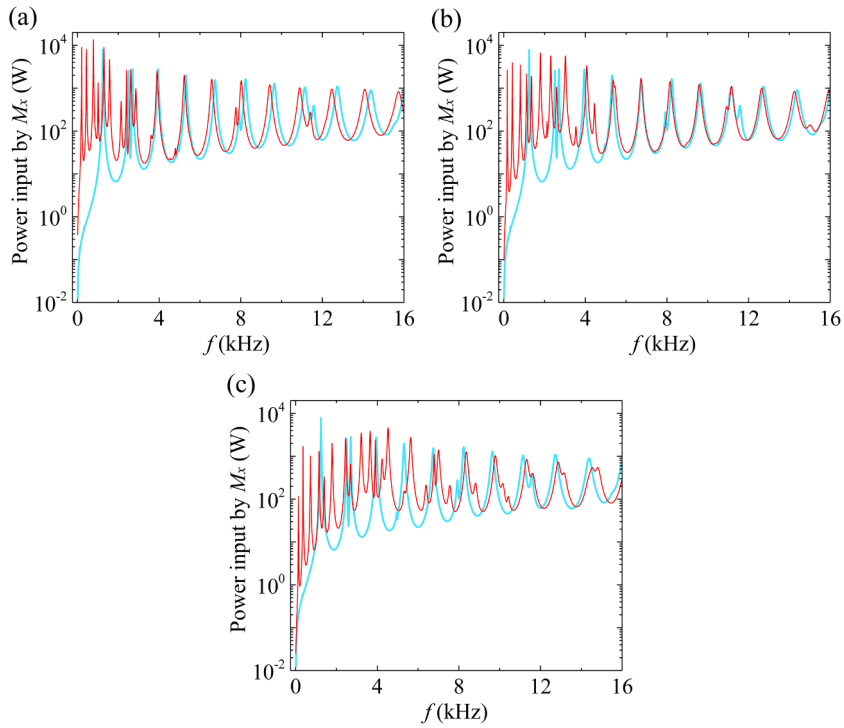


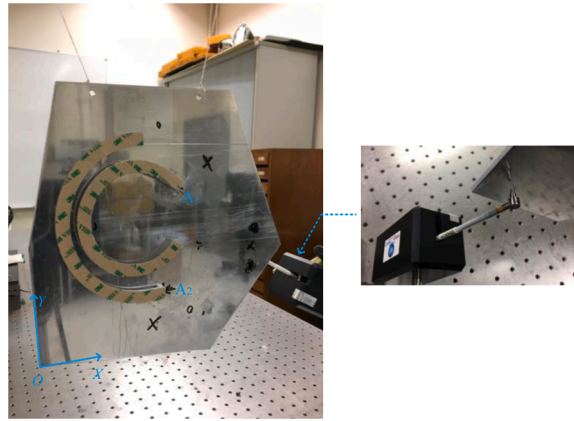
Fig. 4. Spectra of the power input by a unit moment  $M_x$  to the straight ABH (light blue line) and the curved ABHs (a) C-90, (b) C-180 and (c) C-270 (red line).

$$C_T = \left( \frac{GK}{\rho I_p} \right)^{1/2}, \tag{5}$$

where  $GK$  is the torsional rigidity of the bar and  $I_p$  is the second polar moment of the cross-sectional area [41, 42]:

$$K = \frac{BH^3}{16} \left[ \frac{16}{3} - 3.36 \frac{H}{B} \left( 1 - \frac{H^4}{12B^4} \right) \right] \text{ and } I_p = \frac{BH}{12} (B^2 + H^2), \tag{6}$$

with  $B \geq H$ . This expression for  $K$  is found to have a good agreement with the series solution in Ref. [39, 43]. Fig. 3(b) depicts the torsional wave speed at each cross-sectional slice of the ABH wedge, which is calculated with Eq. (5). The accuracy of such an estimation increases with the frequencies. It can be seen that the wave speed decreases with the thickness for a given width and, in the ideal scenario, would also tend to zero when the thickness finally vanishes. An advanced torsional theory by Barr [43], which takes into account the longitudinal stress and the inertia effects, gives more accurate predictions. In most cases the stress correction is more important than the inertia correction. The advanced theory explains the dispersive nature of the torsional waves and the increase of the



**Fig. 5.** ABH absorbers attached on a polygon plate. Damping treatment and attachment locations are also illustrated. The automatic hammer hits the plate back side.

phase velocity with frequencies. More details can be found in the [Appendix A](#). In general, the Saint-Venant theory gives quite good approximation, which is closed to the results from the more accurate advanced theory. Comparing [Figs. 3\(a\)](#) and [\(b\)](#), one can deduce that the decrease of the torsional wavelength along the entire wedge length is greater than that of the flexural waves at a given frequency and the difference in their phase velocities reduces near the thin portion. This is also consistent with the observation from the FEM simulations. Therefore, torsional waves are slowed down as they travel in a wedge with a smoothly reduced thickness profile and their amplitudes increase due to the energy conservation. This results in strong local deformations and enhanced energy concentration, which can eventually be effectively dissipated with damping elements (absent in the current analyses).

To further assess the energy trapping and absorption capability of the ABH module, we calculate the time-average power input to it when a harmonic loading is applied at its thick end. This analysis offers more insights into dynamics of the ABH module and allows to reveal its orientation-dependent properties with respect to the rotational moment excitations  $M_x$  and  $M_y$ , before being added on a two-dimensional plate structure later on. The energy injecting into an ABH component is mainly through dynamic excitations acting on the thick end of each ABH module, namely a transverse force  $F_z$  and rotational moments in two directions  $M_x$  and  $M_y$  (see [Fig. 1](#)). As can be seen, the overall power input to the straight and curved ABHs is quite similar when the applied loading is  $F_z$  or  $M_y$  of one unit in amplitude. We focus on the case when exerting a unit moment  $M_x$ , shown in [Fig. 4](#). Here, the input power  $P_{M_x} = \text{Re}(M_x \psi_x^*) / 2$ , with  $\psi$  representing the angular velocity and the star indicating the complex conjugate. Other conditions are the same as [Fig. 2\(b\)](#). Institively, it is accepted that wedge-like ABHs would not work well with such a rotational excitation.

Under a unit moment excitation  $M_x$ , there is a noticeable difference in the spectra of input power corresponding to the straight and C-shaped ABHs, as shown in [Fig. 4](#). More energy can be admitted by the C-shaped ABHs than the straight one and the ABH with a larger curvature (a lower radius  $R$ ) covers a larger frequency range in terms of energy passage, thus suggesting a better multi-directional performance. The maxima in the power spectra stem from the high responsiveness of the associated resonant modes to the applied loading and these peaks are broadened and become smoother with the increase of frequencies. The resonant torsional wave modes dominate the structural responses of the straight ABH and the lateral bending modes in  $XY$  plane can also be activated. Considering C-shaped ABHs, more modes contribute to the power injection, more pronounced at lower frequencies. The exciting moment  $M_x$  can excite the ABH-type bending modes in addition to the torsional and lateral bending modes. This is owing to the increased geometric irregularity and the breakdown of symmetry results in a coupling of bending-twisting motions [39, 44]. At high frequencies when wavelength becomes shorter, torsional wave modes become dominant and the ABHs C-90 and C-180 respond to the excitation in a similar manner as the straight one. The strong bending-twisting coupling of C-270 can be observed from the results shown in [Fig. 4\(c\)](#). The highly curved ABH shows less orientation-dependant properties. The above analysis echoes the fact that the curvature term  $1/R$  appears in the bending-twisting dynamics of the out-of-plane vibrations in a curved beam, with more details given in [Appendix B](#).

To sum up, the above discussions show that, in addition to the well-known bending wave deceleration, the torsional wave speed also decreases with the thickness thinning in a slender bar with a noncircular cross section. This phenomenon is preserved after curvilinear shape modifications. Compared with the straight ABH design, the planar swirl-shaped ABHs are better at capturing and neutralizing mechanical energy injected by multi-directional rotational excitations. This is attributed to the effective bending and torsional wave compressions and the bending-twisting coupling in a curved ABH-sculpted beam. When adding the curved ABH on a primary structure, the less orientation-dependent dynamic properties are conducive to the energy transfer between the two systems. Meanwhile, the curved ABHs possess enriched dynamics and superior wave trapping effect for energy dissipation, which lead to vibration reductions through structural interaction and damping enhancement effects.

### 3. Experimental studies of ABH absorbers on a plate

Planar swirl-shaped ABH modules are attached on a 2D primary thin structure as add-on vibration control devices. The control

**Table 3**  
Comparisons of different study cases for ABH absorbers

Case	ABH arrangement	Added mass ratio	Gain factor
I	C-270 at $A_1$ and $\gamma = 135^\circ$	3%	39%
II	C-270 at $A_1$ and $\gamma = 135^\circ$ C-180 at $A_2$ and $\gamma = 180^\circ$	6%	63%
III	C-270 at $A_1$ and $\gamma = 135^\circ$ C-180 at $A_2$ and $\gamma = 180^\circ$ C-90 at $A_3$ and $\gamma = 60^\circ$	9%	73%
IV	C-270 at $A'_1$ and $\gamma = -90^\circ$ C-180 at $A'_2$ and $\gamma = -135^\circ$	6%	67%
V	C-270 at $A_1$ and $\gamma = 135^\circ$ C-180 at $A_2$ and $\gamma = 135^\circ$ (back to back attachment)	6%	44%
VI	Coiled ABH at $A'_1$ and $\gamma = -90^\circ$ Coiled ABH at $A'_2$ and $\gamma = -135^\circ$	11.5%	73%

Note: Attachment point coordinates are  $A_1(120, 128)$  mm,  $A_2(100, 37)$  mm,  $A_3(150, 17)$  mm,  $A'_1(107, 180)$  mm and  $A'_2(130, 16)$  mm.

performance and effects of the ABH absorbers are investigated via assessing the measured point responses of the combined system.

### 3.1. System configurations and experimental setup

The primary system is an arbitrarily selected flat polygon plate with no parallel edges, as shown in Fig. 5. The choice was made to represent a general thin structure. The coordinates of the plate vertices in the counter clockwise direction are (0, 0), (151, -31), (240, 61), (180, 210), (27, 210) and (0, 91) mm. The plate is 3mm thick. The position of the driven point is (200, 63) mm. ABH absorbers can be deployed on the plate surface, to be specified for each case later on. The thick end of the ABH absorbers is connected to the host plate through cuboid connectors of dimension  $3 \times 6 \times 10$ mm. Super glue is used for bonding different components. The attachment positions are chosen to be away from the excitation point and plate boundaries. The angle between the starting direction of the ABH baseline (from the thick end to thinner portion) and X-axis is denoted by  $\gamma$ , measured in degrees. The weight of the polygon plate, made of aluminium, is 364g. The plate is drilled with two small penetrated holes and hanged by strings to a rigid frame.

The straight and C-shaped ABHs (C-90, C-180 and C-270) were fabricated according to the geometrical parameter specifications tabulated in Table 1 using also aluminium. Absorbers were made separately from the primary structure, which increases the freedom in terms of choice of design, materials and manufacture methods. The tapered ABH portions were processed through CNC milling. A larger curvature is found to be helpful to improve the static property in terms of structural rigidity/stiffness. For the damping treatment, adhesive tapes 3M<sup>TM</sup> F9473PC were used to coat over the surface of the metal component and a polycoated Kraft liner was retained on the external tape surface to enhance the damping capacities of the soft viscoelastic material. Such a sandwich treatment has been used in Ref. [19] and also considered in other ABH experimental works [45, 46]. The interlayer was built by piling up two thin layers of tapes, with a resultant total thickness of 0.52 mm. The length of the coated damping layer can be optimized if necessary. This, however, is beyond the scope of the present work. A preliminary test was carried out to check the effectiveness of the damping strategy by attaching the treated ABH absorber on the termination of a narrow strip-like waveguide, with 16% the weight of the polygon plate.

A curved ABH in a swirling coil form was also designed and manufactured to test its usability. Such a configuration is more applicable to a structure with a large surface extent. The coiled ABH shown in Fig. 1 was developed by modifying a straight tapered wedge of a length  $L = 420$ mm and a width  $B = 10$ mm. The thickness profile expression is given in Eq. (1) and the maximum and minimum thicknesses are 3.5mm and 0.5mm, respectively. The tapered wedge is divided into 6 parts along the lengthwise direction. Each part, labelled by an integer  $i$  with  $1 \leq i \leq 6$ , is bent into a semi-circle, with corresponding arc radius  $R_i$  decreasing from the thick to thin portions in arithmetic progression. The ABH baseline in a coiled form can be expressed in a parametric equation as

$$x = R_i \sin t, \quad y = R_i \cos t + y_i, \quad (7)$$

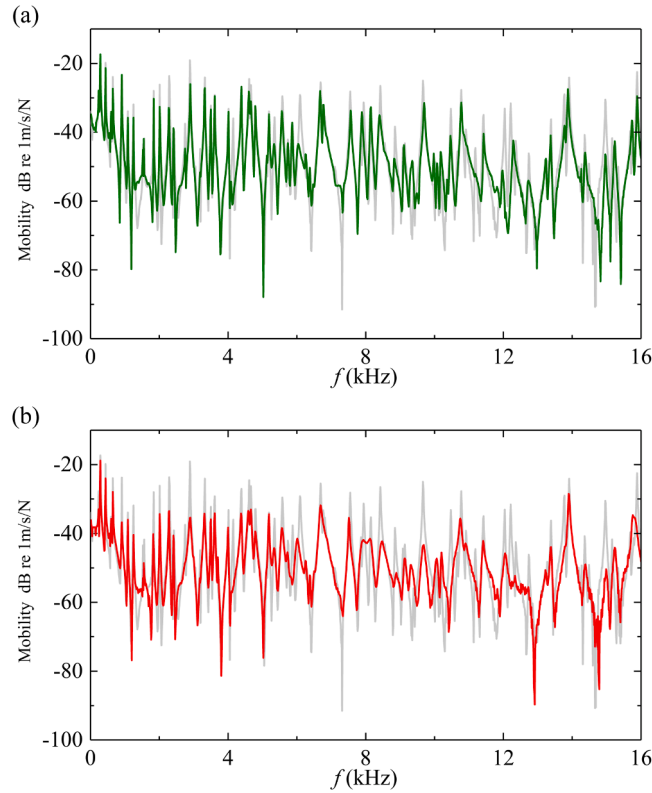
with  $(i-1)\pi \leq t \leq i\pi$  and  $R_i = (7-i)R_6$ . The semi-circle centre is at  $(0, y_i)$ , with  $y_1 = -R_1$  and  $y_{i \geq 2} = (-1)^i R_i + \sum_{n=1}^{i-1} 2(-1)^n R_n$ . The resultant thickness profile is given by  $H(s) = \varepsilon(s-L)^2/L^2 + H_0$ , where  $s$  is the arc length or trajectory. The present coiled ABH is slightly more compact than C-270. To achieve efficient damping effect, only the thinner parts ( $i \geq 3$ ) of the tapered portion are coated with adhesive tapes 3M<sup>TM</sup> F9473PC, consisting of four layers capped by the liner. A uniform portion is extruded from the thick end by 10mm.

The primary plate structure was excited by an automatic hammer system, vImpact-60 from MAUL-THEET<sup>TM</sup>, which allows for simultaneous measurement of the impact force. Structural responses were measured by a Polytec<sup>TM</sup> laser scanning vibro-meter (PSV 400). The distance between the hammer tip and the test plate, as well as the control unit, were carefully adjusted to ensure the quality and the repetitivity of the impact [47]. The acquired temporal force is a typical time pulse over a very short duration and the input spectrum is quite flat within the concerned frequency band. The automatic hammer generates reliable and highly repeatable impact excitations with good coherence confirmed between the excitation and response signals.

### 3.2. Measurement results and discussions

One of the major tasks of the experimental work is to investigate the effectiveness of the planar swirl-shaped ABH absorbers for controlling broadband resonant responses of a general 2D plate structure. To this end, the following part first studies and analyses the control performance when adding an increasing number of C-shaped ABHs to the polygon plate. Investigation is then carried out on the





**Fig. 6.** Driving point mobility of the polygon plate with (a) one curved ABH absorber C-270 (Case I, green line  $\rightarrow$ ) and (b) two curved ABH absorbers, C-180 and C-270 (Case II, red line  $\rightarrow$ ). The grey line  $\text{—}$  is the plate mobility without any absorber.

effect of the attachment positions. Applications of a swirling-coil-type ABH are finally discussed. Altogether 6 cases are tested, labelled from Case I to Case VI. Case specifications are tabulated in Table 3 for easy reference.

Fig. 6(a) shows the driving point mobility of the thin polygon plate before and after one single C-shaped ABH is added. For Case I, an absorber C-270 is installed at point  $A_1(120,128)$  mm (see Fig. 5), with an attachment angle  $\gamma = 135^\circ$  (defined in Section 3.1). The mass ratio between the auxiliary and primary system is  $\mu = 3\%$ . The host structure exhibits typical plate oscillating behaviours, namely numerous very lightly damped resonant peaks appear in a broad frequency range. It can be seen that adding one curved ABH works well only for several resonances and the vibration reduction is not very systematic. It was also found that changing the attachment position did not make a great difference. The reason for this is that only a single ABH, installed at one particular location, is insufficient to absorb enough amount of mechanical energy from the plate.

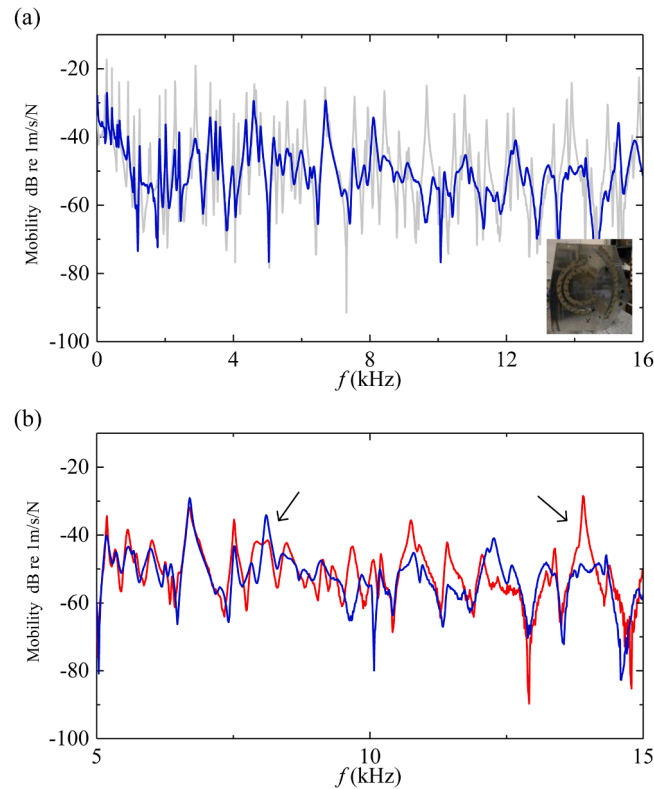
As shown in Fig. 6(b), adding one more curved ABH in Case II, C-180 at  $A_2(100, 37)$  mm with  $\gamma = 180^\circ$ , can lead to apparently more systematic and superior vibration suppression over a broad frequency range. Similar observations were made at other receiver points (not shown here). The attachment positions of the two absorbers are illustrated in Fig. 5 and the added mass ratio  $\mu = 6\%$ . The effectiveness of such a ABH cluster can be seen from the large decrease in the resonance amplitudes and smoothed response curves, resulting from the increase of the overall system loss factors. When attaching two curved ABHs, more vibrational energy in the primary plate enter into the absorbers before getting neutralized, through either DVA or WGA effect [19]. The reverberation effect of flexural waves is found to be notably different. The absorber number and added mass ratio are also important factors in the previous studies on add-on devices like DVA and WGA, see Refs. [26, 33].

To better quantify the vibration reduction level over a prescribed frequency band, we calculate the integral under the square of the velocity response curves at the driving point in the presence and absence of ABH absorbers [26, 48]. Then, a defined Gain factor is obtained by taking the difference of these two integral values normalized to the one without absorber, as

$$G = \frac{\int_0^{f_m} v^2 df - \int_0^{f_m} v_c^2 df}{\int_0^{f_m} v^2 df} \times 100\%, \quad (8)$$

where,  $v$  and  $v_c$  are the velocity responses of the plate without and with absorbers, respectively; and  $f_m$  the maximum frequency for evaluation. The Gain factors over the entire frequency band for Cases I and II are 39% and 63%, respectively. Comparisons from other subsequent cases studied in this section are summarized in Table 3.

Increasing the number of absorbers to three (Case III) can further reduce the plate response level and increase the full-band Gain

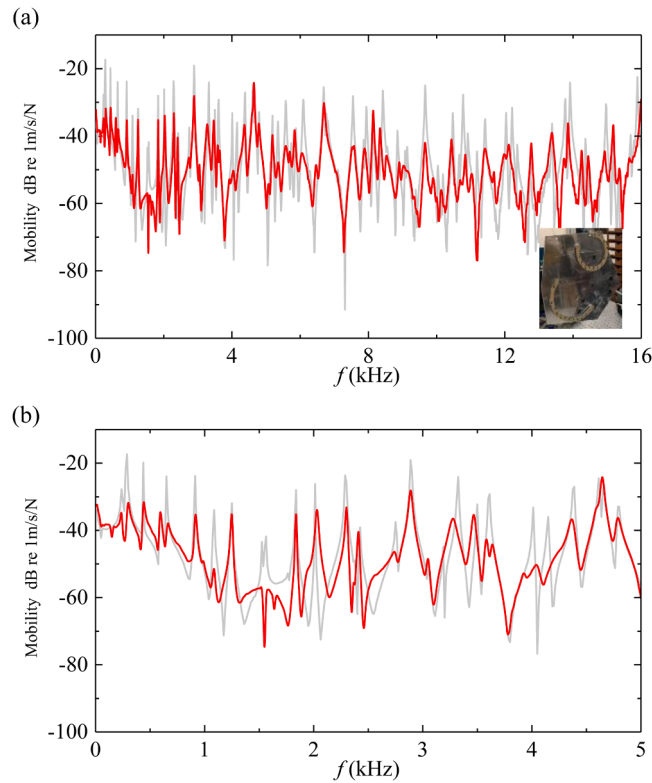


**Fig. 7.** Comparisons of the driving point mobility of the Case III using three curved ABH absorbers, C-90, C-180 and C-270 (blue line —) with (a) the case using no absorber (grey line —) and (b) Case II using two absorbers, C-180 and C-270 (red line —). Arrows in mark the positive or adverse effects of the mutual interaction in a system containing multiple ABH absorbers.

factor to 73%, as shown in Fig. 7 (a). The third absorber C-90 is located at  $A_3(150, 17)$  mm, with  $\gamma = 60^\circ$  and the total added mass ratio reaches to  $\mu = 9\%$ . The new ABH cluster takes effect for most structural resonances. One can notice that the ABH cluster also positively impact the low-frequency vibration by obvious reduction in the level, compared to the case with two ABHs. The Gain factor below 2000Hz is improved from 43% to 68%. Such a benefit is also observed at other positions (not shown here). Recall that the fundamental frequency of the straight ABH in the numerical analyses is 111Hz, which is close to those of the C-shaped ABHs. The first vibration resonance frequency of the polygon plate is 237.5Hz. When comparing the plate responses of Case II using two absorbers and Case III using three absorbers in Fig. 7 (b), most peaks are further attenuated near original resonance frequencies due to the improved energy loss. It can be found that mutual interaction effects in a system containing multiple ABH absorbers can promote or compromise the control effects simultaneously (indicated by the arrows). Nevertheless, the deployment of more ABH absorbers can generally enhance the vibration suppression and ensure performance robustness, owing to the multi-directional and efficient wave absorbing effects.

The effect of the attachment position is then investigated. Fig. 8 gives the response of the combined system after re-arranging the installation positions of two absorbers C-180 and C-270 in Case II (Fig. 5). In this new case, referred to as Case IV, C-270 is at  $A'_1(107, 180)$  mm with  $\gamma = -90^\circ$  and C-180 is at  $A'_2(130, 16)$  mm with  $\gamma = -135^\circ$ . It can be seen that the ABH cluster with a different arrangement still shows effectiveness in coping with plate resonant responses, with a full-band Gain factor 67% close to previous arrangement. This further demonstrates the robustness of the proposed ABH absorbers. This also results in an improvement in low-frequency performance, as shown in Fig. 8(b), with Gain factor below 2000Hz being 72%. The vibration suppression effect of the C-shaped ABH absorbers obviously depends on their attachment positions, particularly in a low-frequency range where vibrational energy distribution over the plate is less uniform. This leaves the room and calls for more meticulous adjustment of the absorber installation, in agreement with studies on conventional vibration control devices [31, 32]. A clear peak splitting phenomenon, typical of strong dynamic absorber effects, appears around 3.6kHz (see Fig. 8(b)) and other resonant peaks are heavily smoothed or reduced near the original resonances. The typical control effects by add-on ABHs, dominated by structural interaction and damping enhancement, are observed from the mobility curves. The curved ABH absorbers still possess enriched dynamics and enhanced damping, just as the straight ABH, and embraces the working principles of DVA and WGA.

A further experimental measurement (Case V) was carried out to move the ABH C-180 in Case II of Fig. 5 to the same attachment position  $A_1$  and angle  $\gamma$  as C-270, but on opposite sides of plate. It was found that this back-to-back attachment results in a poor control effect, which is comparable with case I using only one absorber C-270 in Fig. 6(a) with a close full-band Gain factor. This indicates that a decentralized or distributed arrangement is a better option for the enhancement of the energy transfer between an auxiliary add-on



**Fig. 8.** Driving point mobility of a polygon plate with two ABH absorbers attached at different positions (Case IV, red line  $\rightarrow$ ). The grey line  $\text{—}$  is the plate mobility without any attachment. (b) is the response in a narrow frequency range of (a).

device and a multi-modal thin structure.

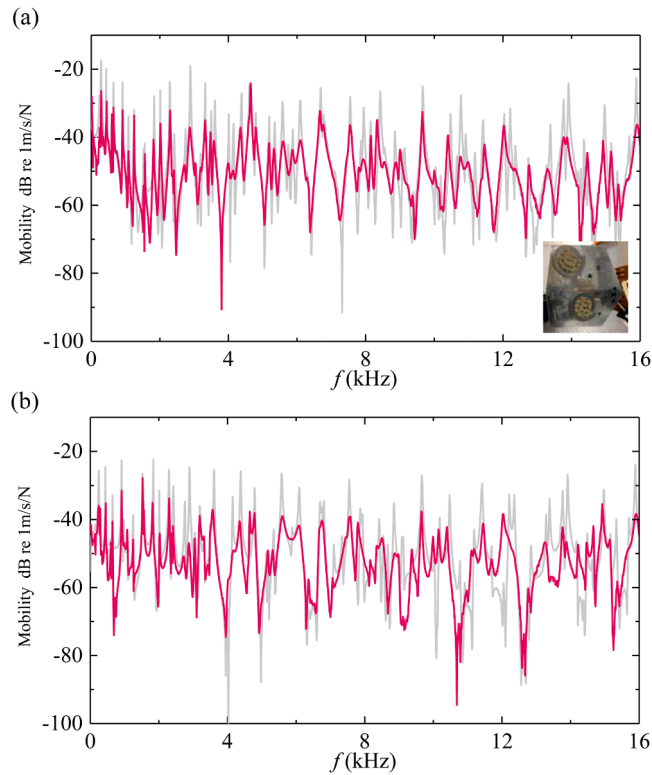
As a final verification, coiled ABHs are deployed to demonstrate their control effectiveness and robustness. Fig. 9 shows the driving and cross point responses of Case VI when two coiled ABHs are added in the same way as Case IV. A high full-band Gain factor of 73% is obtained with a total added weight ratio  $\mu = 11.5\%$ . The measured results further illustrate the generality of vibration suppressing phenomenon brought by add-on curved ABHs. Such a swirl coil form is more applicable for thin structures with larger spans. The control efficiency can be further improved by optimizing the ABH design, such as extending the thin tip by a platform [29], adopting a variable width [21] or using other 3D geometric features [24, 25, 49].

#### 4. Conclusions

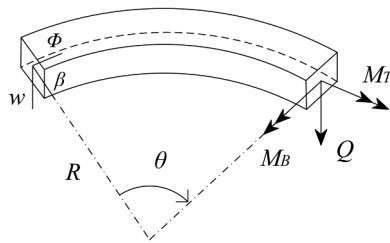
In this work, we propose a planar swirl-shaped ABH absorber as a compact, multi-directional and scalable vibration-suppressing device without resorting to a delicate parameter tuning process. The absorber, embracing the working principles of both DVA and WGA, is shown to entail broadband and multi-directional vibration suppressions for a vibrating structure.

The observed multi-directional vibration suppression performance originates from the swirl-shaped ABH design, which enables rich distributed resonant modes, effective bending-twisting coupling and high system loss inside the absorbers. It is shown that, in addition to the widely explored bending waves, torsional waves can also be slowed down during their propagation towards the thin structural part with non-circular cross sections. Owing to these wave compression effects and the bending-twisting coupling, the curved ABH beams exhibit superior dynamic properties in capturing and neutralizing energy injected through multi-directional rotational excitations, which ameliorates with the increase of the curvature. The combined benefit of the curvilinear ABH design is the provision of a new set of ABH-based vibration absorbers, which, empowered by the aforementioned properties, offers enriched dynamic coupling with a primary system to maximize the most silent ABH features for vibration control applications.

Experimental studies demonstrate the practicability and the effectiveness of the proposed ABH absorbers for suppressing broadband vibrations of a general thin structure, exemplified by a polygon plate. The deployment of multiple ABH-tailored absorbers (or an ABH cluster) can guarantee robust vibration control performance, which improves with the absorber number. Considerable resonant peak reductions are achieved using the same ABH cluster with different spatial arrangements. Resonant peaks of the host structure can be reduced through structural interaction with the absorbers (typical of DVA effect) or damping enhancement (typical of WGA effect). The occurrence of such physical process is made easier by the enriched dynamics and remarkable wave trapping ability of the absorbers brought by the curvilinear ABH design. Experimental tests on the final swirling coil configuration illustrate the efficacy and the practical outlook of the proposed ABH absorber.



**Fig. 9.** (a) Driving and (b) cross point mobility of a polygon plate with two coiled ABH absorbers (Case VI, pink line —), attached in the same way as Fig. 8. The cross point response is measured at (154, 152) mm. The grey line — is the plate mobility without any attachment.



**Fig. 10.** A planar curved beam element in a circular arc form.

As a final remark, one should note the general vibration control strategy proposed in this work is not limited to a particular structural configuration. The idea can be extended to more complex engineering structures. It is also relevant to mention that while most existing works focus on black hole effects for flexural waves and sonic waves [1], this study uncovers similar deceleration phenomena for torsional waves in a tapered bar with non-circular cross sections, which may trigger new interests and impetus to future ABH studies and applications.

**CRedit authorship contribution statement**

**Tong Zhou:** Conceptualization, Methodology, Investigation, Writing – original draft. **Li Cheng:** Investigation, Supervision, Writing – review & editing.

**Declaration of Competing Interest**

The authors declare that they have no known competing financial interests or personal relationships that could have appeared to influence the work reported in this paper.

**Acknowledgments**

The authors are grateful to Mr. Thomas Tang from the Hong Kong Polytechnic University and Mr. Qing Li and Dr. Su Zhang from Midea group for helping manufacture the curved ABH beam samples used in experiments.

**Appendix A. Barr’s advanced torsional theor**

Reference [43] presents a 4th-order differential equation for torsional vibrations in a rod with a rectangular cross section. After appropriate substitutions, the torsional wave speed at a given frequency can be obtained by solving the following equation:

$$\left[ \frac{\rho^2}{EG} - \frac{(1-\kappa)\rho}{\tau^2 E \omega^2} \right] C_T^4 + \left[ \frac{\kappa(1-\kappa)G}{\tau^2 E \omega^2} - \left( \frac{\rho}{G} + \frac{\rho \alpha^2}{E} \right) \right] C_T^2 + \alpha^2 = 0. \tag{A.1}$$

Here,  $\kappa$  and  $\tau$  are the shape constants factors:

$$\kappa = \frac{4H^2}{B^2 + H^2} \left( 1 - \frac{192H}{\pi^2 B} \sum_{i=1,3,5,\dots}^{\infty} \frac{1}{i^5} \tanh \frac{i\pi B}{2H} \right), \tag{A.2}$$

with  $\kappa = K/I_p$  (see E.q (6)) and

$$\tau^2 = \frac{H^4}{B^2 + H^2} \left[ \frac{B^2}{3H^2} + \frac{768}{\pi^6} \sum_{i=1,3,5,\dots}^{\infty} \frac{1}{i^6} \left( \frac{3 \tanh i\pi B / 2H}{i\pi B / 2H} + \tanh^2 i\pi B / 2H - 3 \right) \right], \tag{A.3}$$

where the constant  $\alpha^2 = 0.86$  for the material Poisson’s ratio being 0.3. The lower branch of the solutions to Eq. (A.1) corresponds to the phase velocities of torsional waves. The validity of the wave velocity evaluation can be checked by calculating the eigenfrequencies of a free-free finite uniform bar of length  $L$

$$\left( \frac{\omega}{\omega_s} \right)^4 - \left[ \frac{E + G\alpha^2}{G\kappa} + \frac{1 - \kappa}{\kappa(\tau n\pi/L)^2} \right] \left( \frac{\omega}{\omega_s} \right)^2 + \frac{E\alpha^2}{G\kappa^2} + \frac{1 - \kappa}{k(\tau n\pi/L)^2} = 0 \tag{A.4}$$

where  $n$  is an integer and  $\omega_s$  the eigenfrequency of the same bar predicted by the Saint-Venant theory

$$\omega_s = \sqrt{\frac{G\kappa}{\rho}} \frac{n\pi}{L}, \tag{A.5}$$

The smaller value given by Eq. (A.4) for a given  $n$  is of interest while the larger one is trivial. By using free bars of finite lengths and different dimensions, both Saint-Venant and Barr models for torsional vibrations used in this work were validated through comparing the eigen-frequencies calculated by the theoretical methods and FEM, similar with Refs. [42, 43].

**Appendix B. Bending-twisting coupling of a curved beam**

The bending-twisting coupling in the swirl-shaped ABHs can be analysed by resorting to a uniform planar curved beam element [44, 50], as shown in Fig. 10. The equations of motion for the out-of-plane vibration of a curved beam or a circular ring write

$$Q' = \rho S \ddot{w}, \tag{B.1}$$

$$M'_B + \frac{M_T}{R} - Q = \rho I \ddot{\beta}, \tag{B.2}$$

$$M'_T - \frac{M_B}{R} = \rho I_p \ddot{\phi}, \tag{B.3}$$

These equations of motions include shear deformations and rotary inertia effects. Here, the prime donates the derivative with respect to arc length  $s = \theta R$  and the dot represents the time derivative. The structural deformations are described by the transverse displacement  $w$ , bending rotation  $\beta$  and twisting rotation  $\phi$  of the cross section. The transverse force  $Q$ , bending moment  $M_B$  and twisting moment  $M_T$  can be expressed as

$$Q = kGA(w' + \beta), \tag{B.4}$$

$$M_B = EI \left( \beta' + \frac{\phi}{R} \right), \tag{B.5}$$

$$M_T = GK \left( \phi' - \frac{\beta}{R} \right). \tag{B.6}$$

Here,  $k$  is the shear correction factor [50]. It can be seen from above equations that the bending-twisting coupling of a curved beam depends on the curvature radius  $R$  and the twist angle  $\phi$  is related to flexural motion (displacement  $w$  and rotation  $\beta$ ). If  $R$  tends to infinity, Eq. (B.1) and (B.2) degenerate to Timoshenko beam bending equations and Eq. (B.3) retreats to the equation of motion of the simple theory for torsional vibrations, indicating that the bending and twisting vibrations are decoupled.

## References

- [1] A. Pelat, F. Gautier, S.C. Conlon, F. Semperlotti, The acoustic black hole: A review of theory and applications, *J. Sound Vib.* 476 (2020), 115316.
- [2] M.A. Mironov, Propagation of a flexural wave in a plate whose thickness decreases smoothly to zero in a finite interval, *Soviet Phys.: Acoustics* 34 (3) (1988) 318–319.
- [3] V.V. Krylov, Acoustic black holes: recent developments in the theory and applications, *IEEE T. Ultrason. Ferr.* 61 (8) (2014) 1296–1306.
- [4] V.V. Krylov, F.J.B.S. Tilmann, Acoustic ‘black holes’ for flexural waves as effective vibration dampers, *J. Sound Vib.* 274 (3) (2004) 605–619.
- [5] V. Denis, A. Pelat, F. Gautier, B. Elie, Modal overlap factor of a beam with an acoustic black hole termination, *J. Sound Vib.* 333 (12) (2014) 2475–2488.
- [6] A. Karlos, S.J. Elliott, J. Cheer, Higher-order WKB analysis of reflection from tapered elastic wedges, *J. Sound Vib.* 449 (2019) 368–388.
- [7] J. Leng, V. Romero-García, A. Pelat, R. Picó, J.P. Groby, F. Gautier, Interpretation of the Acoustic Black Hole effect based on the concept of critical coupling, *J. Sound Vib.* 471 (2020), 115199.
- [8] M. Ouisse, D. Renault, P. Butaud, E. Sadoulet-Reboul, Damping control for improvement of acoustic black hole effect, *J. Sound Vib.* 454 (2019) 63–72.
- [9] L. Tang, L. Cheng, Periodic plates with tunneled Acoustic-Black-Holes for directional band gap generation, *Mec. Syst. Sig. Process.* 133 (2019), 106257.
- [10] Y. Zhang, K. Chen, S. Zhou, Z. Wei, An ultralight phononic beam with a broad low-frequency band gap using the complex lattice of acoustic black holes, *Appl. Phys. Express* 12 (7) (2019), 077002.
- [11] N. Gao, X. Guo, B. Cheng, Y. Zhang, Z. Wei, H. Hou, Elastic Wave Modulation in Hollow Metamaterial Beam With Acoustic Black Hole, *IEEE Access* 7 (2019) 124141–124146.
- [12] P.A. Feurtado, S.C. Conlon, Wavenumber transform analysis for acoustic black hole design, *J. Acoust. Soc. Am.* 140 (1) (2016) 718–727.
- [13] L. Ma, L. Cheng, Sound radiation and transonic boundaries of a plate with an acoustic black hole, *J. Acoust. Soc. Am.* 145 (1) (2019) 164–172.
- [14] L. Zhang, G. Kerschen, L. Cheng, Electromechanical Coupling and Energy Conversion in a PZT-Coated Acoustic Black Hole Beam, *Int. J. Appl. Mech.* 12 (08) (2020), 2050095.
- [15] J. Deng, O. Guasch, L. Zheng, T. Song, Y. Cao, Semi-analytical model of an acoustic black hole piezoelectric bimorph cantilever for energy harvesting, *J. Sound Vib.* 494 (2021), 115790.
- [16] H. Ji, Y. Liang, J. Qiu, L. Cheng, Y. Wu, Enhancement of vibration based energy harvesting using compound acoustic black holes, *Mec. Syst. Sig. Process.* 132 (2019) 441–456.
- [17] C.A. McCormick, M.R. Shepherd, Design optimization and performance comparison of three styles of one-dimensional acoustic black hole vibration absorbers, *J. Sound Vib.* 470 (2020), 115164.
- [18] L. Ma, H.-W. Dong, L. Cheng, An alternative and optimized thickness profile of an acoustic black hole plate, *J. Sound Vib.* 486 (2020), 115619.
- [19] T. Zhou, L. Cheng, A resonant beam damper tailored with Acoustic Black Hole features for broadband vibration reduction, *J. Sound Vib.* 430 (2018) 174–184.
- [20] J.I. Daniel, *Engineering vibration*, Prentice-Hall, Inc., New Jersey, 2001.
- [21] E.E. Ungar, L.G. Kurzweil, *Preliminary Evaluation of Waveguide Vibration Absorbers*, Bolt Beranek and Newman Inc Cambridge Ma, 1984.
- [22] T. Zhou, L. Tang, H. Ji, J. Qiu, L. Cheng, Dynamic and static properties of double-layered compound acoustic black hole structures, *Int. J. Appl. Mech.* 9 (05) (2017), 1750074.
- [23] C. Zhao, M.G. Prasad, Acoustic Black Holes in Structural Design for Vibration and Noise Control, *Acoustics* 1 (1) (2019) 220–251.
- [24] J.Y. Lee, W. Jeon, Vibration damping using a spiral acoustic black hole, *J. Acoust. Soc. Am.* 141 (3) (2017) 1437–1445.
- [25] S.-Y. Kim, D. Lee, Numerical simulation of characteristics of wave propagation and reflection coefficient in a helix-acoustic black hole, *J. Vib. Control* (2020).
- [26] D.J. Mead, *Passive vibration control*, John Wiley & Sons Inc, 1998.
- [27] A. Carvalho de Sousa, E. Deckers, C. Claeys, W. Desmet, On the assembly of Archimedean spiral cavities for sound absorption applications: Design, optimization and experimental validation, *Mec. Syst. Sig. Process.* 147 (2021), 107102.
- [28] T. Durand-Texte, A. Pelat, G. Penelet, F. Gautier, M. Sécail-Géraud, Thermal imaging of the structural damping induced by an acoustic black hole, *J. Appl. Phys.* 127 (2) (2020), 025102.
- [29] L. Tang, L. Cheng, Enhanced Acoustic Black Hole effect in beams with a modified thickness profile and extended platform, *J. Sound Vib.* 391 (2017) 116–126.
- [30] B.G.E. Korenev, L.M. Reznikov, *Dynamic vibration absorbers: theory and technical applications*, John Wiley & Sons, 1993.
- [31] C. Yang, D. Li, L. Cheng, Dynamic vibration absorbers for vibration control within a frequency band, *J. Sound Vib.* 330 (8) (2011) 1582–1598.
- [32] C.M. Pray, S.A. Hambric, T.E. McDevitt, C.B. Burroughs, Characterization of folded beam waveguide absorbers for damping of flexural vibrations in a thick plate, *Noise Control Eng. J.* 48 (6) (2000) 185–192.
- [33] S.J. Watson, *Experimental studies of circular viscoelastic waveguide absorbers for passive structural damping*, Monterey, California, Naval Postgraduate School (1989).
- [34] H. Ji, N. Wang, C. Zhang, X. Wang, L. Cheng, J. Qiu, A vibration absorber based on two-dimensional acoustic black holes, *J. Sound Vib.* 500 (2021), 116024.
- [35] S. Park, M. Kim, W. Jeon, Experimental validation of vibration damping using an Archimedean spiral acoustic black hole, *J. Sound Vib.* 459 (2019), 114838.
- [36] J.Y. Lee, W. Jeon, Wave-based analysis of the cut-on frequency of curved acoustic black holes, *J. Sound Vib.* 492 (2021), 115731.
- [37] T. Zhou, J.D. Chazot, E. Perrey-Debain, L. Cheng, Partition of Unity Finite Element Method for the modelling of Acoustic Black Hole wedges, *J. Sound Vib.* 475 (2020), 115266.
- [38] K. Hook, J. Cheer, S. Daley, A parametric study of an acoustic black hole on a beam, *J. Acoust. Soc. Am.* 145 (6) (2019) 3488–3498.
- [39] J.S. Rao, *Advanced theory of vibration (Nonlinear vibration and one dimensional structures)*, Halsted Press, 1992.
- [40] M. Petyt, *Introduction to finite element vibration analysis*, Cambridge university press, 2010.
- [41] A.W. Leissa, M.S. Qatu, *Vibrations of continuous systems*, McGraw-Hill, New York, 2011.
- [42] D. A. Russell. *Torsional Vibrations in Free-Free Bar with Rectangular Cross-Section*. (2018) Available: <https://www.acs.psu.edu/drussell/Demos/Torsional/torsional.html>.
- [43] A.D.S. Barr, Torsional Waves in Uniform Rods of non-Circular Section, *J. Mech. Eng. Sci.* 4 (2) (1962) 127–135.
- [44] P. Chidamparam, A.W. Leissa, Vibrations of Planar Curved Beams, Rings, and Arches, *Appl. Mech. Rev.* 46 (9) (1993) 467–483.
- [45] J. Deng, L. Zheng, P. Zeng, Y. Zuo, O. Guasch, Passive constrained viscoelastic layers to improve the efficiency of truncated acoustic black holes in beams, *Mec. Syst. Sig. Process.* 118 (2019) 461–476.
- [46] T. Durand-Texte, A. Pelat, G. Penelet, F. Gautier, M. Sécail-Géraud, Thermal imaging of vibrational energy dissipated in a 2D acoustic black hole pit, *Appl. Phys. Lett.* 118 (1) (2021), 013901.
- [47] P. Avitabile, Experimental modal analysis, *Sound Vib* 35 (1) (2001) 20–31.

- [48] L. Cheng, R. Lapointe, Vibration attenuation of panel structures by optimally shaped viscoelastic coating with added weight considerations, *Thin-walled structures* 21 (4) (1995) 307–326.
- [49] L. Zhao, S.C. Conlon, F. Semperlotti, Broadband energy harvesting using acoustic black hole structural tailoring, *Smart Mater. Struct.* 23 (6) (2014), 065021.
- [50] S.S. Rao, *Vibration of Continuous Systems*, John Wiley & Sons, Hoboken, N.J., 2007.